Topology Study of Photovoltaic Interface for Maximum Power Point Tracking

Weidong Xiao, *Student Member, IEEE*, Nathan Ozog, *Student Member, IEEE*, and William G. Dunford, *Senior Member, IEEE*

***Abstract*—This paper looks at the performance of photovoltaic modules in nonideal conditions and proposes topologies to minimize the degradation of performance caused by these conditions. It is found that the peak power point of a module is significantly decreased due to only the slightest shading of the module, and that this effect is propagated through other nonshaded modules connected in series with the shaded one. Based on this result, two topologies for parallel module connections have been outlined. In addition, dc/dc converter technologies, which are necessary to the design, are compared by way of their dynamic models, frequency characteristics, and component cost. Out of this comparison, a recommendation has been made.**

***Index Terms*—DC–DC power conversion, modeling, photovoltaic power systems, topology, voltage control.**

I. Introduction

PHOTOVOLTAIC power is an established technology and has recently experienced rapid growth over the last ten years [1]. Photovoltaic cells are the key component in most photovoltaic power systems, but their performance is still subpar, so future work is needed to improve their performance and optimize the interactions between the cells and other components. The purpose of this paper is to investigate how to improve the control of the power interface and optimize the operation of the overall system.

In a 24-h day, sunlight is only available for a limited time and depends heavily on weather conditions. In most photovoltaic power systems, a particular control algorithm, namely maximum power point tracking (MPPT), is utilized to take full advantage of the available solar energy. Thus, the direction of this paper is to develop topologies for MPPT systems in order to more efficiently use harvested solar energy.

Two principal types of photovoltaic power systems exist, which are classified by their functions and configuration, namely: 1) stand-alone systems and 2) grid-connected systems [2]–[6]. The operation of stand-alone photovoltaic systems is independent of the electric utility grid. Recently, there have been an increasing number of grid-connected systems, which are in parallel with the electric utility grid and supply solar power to the utility via the grid. Ninety-three percent of the solar power systems installed in 2004 are grid-connected structures [1]. The operation of MPPT is to adjust photovoltaic interfaces so that the operating characteristics of the load and the photovoltaic array match at the maximum power point (MPP) no matter what the stand-alone or grid-connected photovoltaic application, which are numerous.

This paper first investigates how partial shading affects the performance of MPPT and solar power generation. Second, it discusses topologies used for the optimization of MPPT of photovoltaic power systems. This paper presents two system structures suitable for photovoltaic features and MPPT. Finally, it gives a comparative study to select the best converter topology for photovoltaic interfaces.

Manuscript received October 16, 2006; revised January 29, 2007.

The authors are with the University of British Columbia, Vancouver, BC V6T 1Z4, Canada (e-mail: weidongx@ece.ubc.ca).

Color versions of one or more of the figures in this paper are available online at http://ieeexplore.ieee.org.

Digital Object Identifier 10.1109/TIE.2007.894732

II. Nonideal Conditions of Photovoltaic Power Generation

Nonideal conditions refer to some specific situations where solar cells reach their limits and cannot provide specified power. The problem, which is referred to in some literatures as "nonoptimal conditions" or "unbalanced generations," has drawn recent attention [7]–[13]. Common nonideal conditions include partial shading, low solar radiation, dust collection, and photovoltaic ageing. The following paragraphs address the major effects, which result from partial shading.

Generally, it is preferable to build a solar array using all the same panels and to keep them away from any shading. However, it is not easy to avoid shading in residential installations because of the change in sunlight direction throughout the day. Furthermore, obstacles, such as trees, birds, and other constructions, etc., can cause partial shading. Studies [11] have revealed that minor shading can cause a major reduction in solar power output of the photovoltaic array.

In this paper, an experiment was conducted to quantify the consequence of shading in photovoltaic power systems. Fig. 1 shows two identical photovoltaic BP350 modules, which were installed on the same frame in the same direction and at the same angle on a roof, allowing them to be tested at the same time and under the same conditions. Each BP350 module is comprised of 72 photovoltaic cells, as described in [14]. The data acquisition system was configured to simultaneously record the outputs of both photovoltaic modules.

The experiment first tested and calibrated the current–voltage (I–V) curves of two photovoltaic modules under the same environmental conditions. The system was then reconfigured to measure the output characteristics when one cell was intentionally shaded. Again, the I–V curves of two photovoltaic modules were measured simultaneously while one of the two

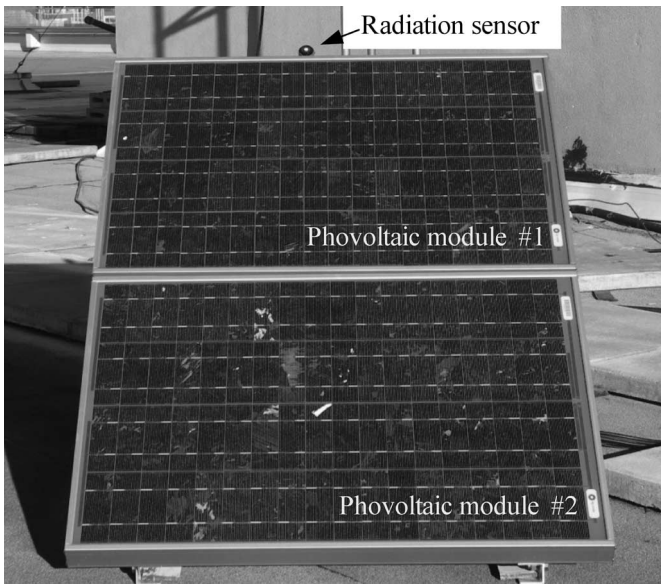

Fig. 1. Two photovoltaic modules installed on one frame at the same angle and direction.

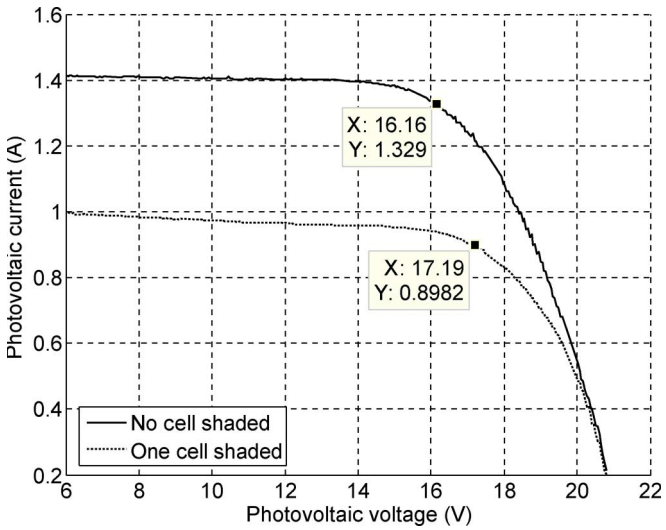

Fig. 2. Measured I–V curves of one-cell-shaded and nonshaded modules.

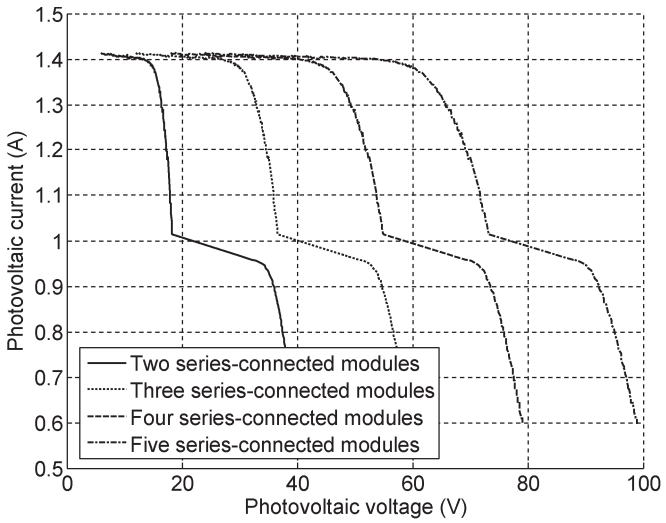

Fig. 3. Measured I–V curves when the one-cell-shaded module is series connected with the other nonshaded modules.

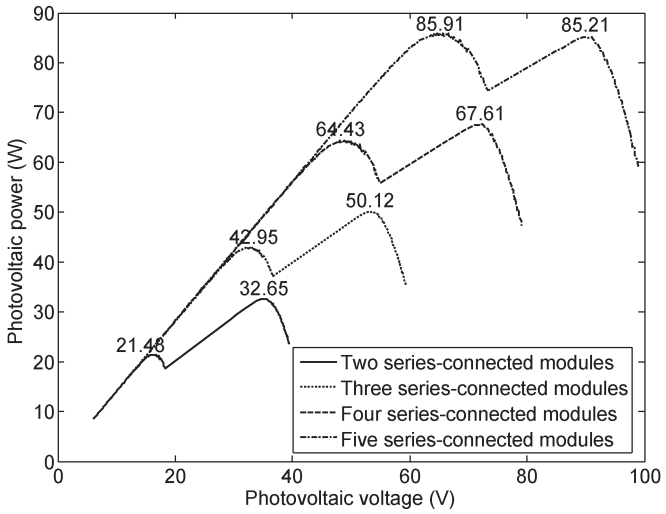

Fig. 4. Measured P–V curves when the one-cell-shaded module is serially connected to other nonshaded modules.

modules was partially shaded. The different output characteristics of the one-cell-shaded module and the nonshaded module are shown in Fig. 2 with their I–V curves. As illustrated, the peak power point degrades to 15.44 W from 21.48 W when one of the 72 cells is shaded. When the shaded module is series connected with other nonshaded modules, an additional loss occurs; this is discussed in the following paragraphs.

The output characteristics when the one-cell-shaded photovoltaic module is connected to other nonshaded modules in series are illustrated in Figs. 3 and 4. In most photovoltaic modules, the cells are connected in series for specific output voltages. The shading effect results in degraded module output because the current of the series-connected string in modules is affected by the shaded cell. Investigations [11] have been conducted to evaluate the effects of shading on module and array performance. This has resulted in module manufacturers employing bypass diodes to preserve array voltage and to minimize hot-spot heating and the potential for cell failures when shaded. The significant losses caused by a series-connected structure under this condition are tabulated in Table I. In some cases, the bypass diode can reduce performance degrading, as shown in Table I and Fig. 4, when the one-cell-shaded module is series connected with four nonshaded modules. When the diode conducts to bypass the shaded cell string, the peak power becomes 85.91 W, which is higher than the value (85.21 W) when all cell strings work together. This is to say that it is more efficient to completely remove the compromised cell than to have it operate at partial capacity and degrade the performance of the other cells in its string.

The paper finds that the shaded cell contributes a 14.06% power loss, and an additional 11.57% loss results from reduced MPP when the two modules are connected in series. When three or more modules are series connected, the situation is even worse, as summarized in Table I. Fig. 4 also illustrates that there are two peak power points in the P–V curves due to the shading condition. None of the peak points represent the

TABLE I
LOSSES CAUSED BY SERIES-CONNECTED MODULES UNDER ONE-CELL-SHADED CONDITION

Connections	Hidden MPP	Achievable MPP	Relative Losses (%)
Two series-connected modules	36.92W	32.65W	11.57%
Three series-connected modules	58.40W	50.12W	14.18%
Four series-connected modules	79.88W	67.61W	15.36%
Five series-connected modules	101.36W	85.91W	15.24%

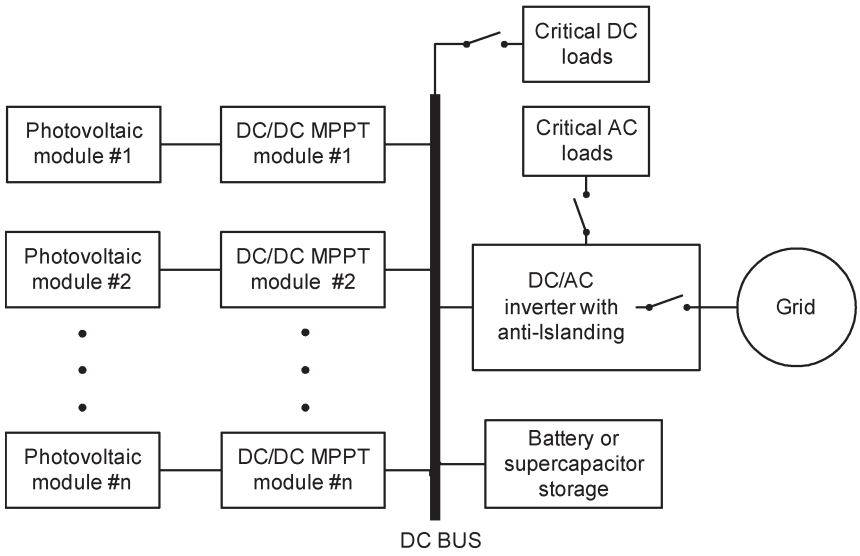

Fig. 5. Topology of grid-connected photovoltaic power systems with a dc bus and a UPS function.

true optimal operating condition, which is equal to the sum of the individual maximum power of each photovoltaic module. So far, the discussion has been based on the one-cell-shaded situation. The shading condition could be more complicated in practical photovoltaic applications, making it more difficult to perform MPPT.

To increase the conversion efficiency, some popular inverter designs [15], [16] tend to the series configurations of photovoltaic modules to obtain a moderate-voltage dc source (i.e., 200 V). This requires at least 300 solar cells in series connection. For these systems, the nonideal effect would clearly be critical.

III. SYSTEM STRUCTURE

The previous section demonstrates that nonideal conditions considerably degrade the performance of MPPT, especially when photovoltaic modules are connected in series. To alleviate the complexity caused by interconnecting photovoltaic modules, this paper recommends an individual power interface for each photovoltaic module. One grid-connected topology is proposed and illustrated in Fig. 5. In this configuration, defective modules do not degrade the performance of other modules, which means that the overall system is only impacted to the extent that the single degraded module affects it.

The dc/dc MPPT modules track the MPPs of photovoltaic modules and deliver power to the dc bus. Solar energy is eventually transferred to the grid via a centralized dc/ac inverter with the anti-islanding function. The anti-islanding device constantly senses the grid status and the power quality of solar generation. It connects the photovoltaic power system to the grid when the system is in a normal operation and is able to disconnect the system from the grid to avoid any islanding problems, as described in [17] and [18]. This configuration has the flexibility to be added to an uninterruptible power supply (UPS) function when some storage devices such as batteries and/or super capacitors are installed, as shown in Fig. 5. During blackouts, the electricity can be continuously supplied to the critical loads by both the storage units and the photovoltaic modules. To simplify the analysis, the block diagram shown in Fig. 5 ignores a charge and discharge interface for the storage devices. This is necessary to keep the normal charge or discharge cycle between the storage unit and dc voltage bus. To limit the scope of the analysis, only the interface of the dc/dc MPPT module is designed and investigated in the following studies.

IV. CONTROL VARIABLES OF MPPT

Different from the applications of space programs, significant radiation power is filtered and blocked by the atmosphere and cloud cover before it is received at the earth surface, which dramatically affects the available insolation for photovoltaic generators. Changes in these variables cause the I–V curves and MPPs of photovoltaic modules to change as well, as illustrated in Fig. 6, where Ga symbolizes the solar insolation. Besides insolation, another important factor influencing the characteristics of a photovoltaic module is cell temperature, as shown in Fig. 7. The cell temperature variation causes the MPP to change significantly along the x-axis. Fig. 8 illustrates the temperature effect based on the relationship of power and

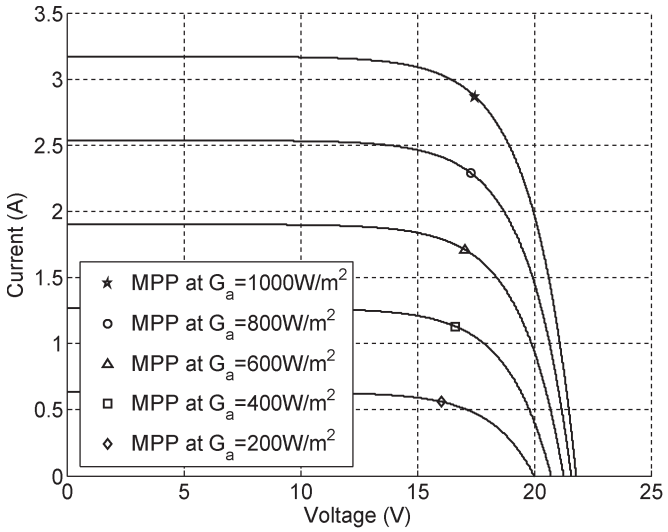

Fig. 6. Simulated I–V curves of BP350 influenced by insolation when the cell temperature is constant 25 °C.

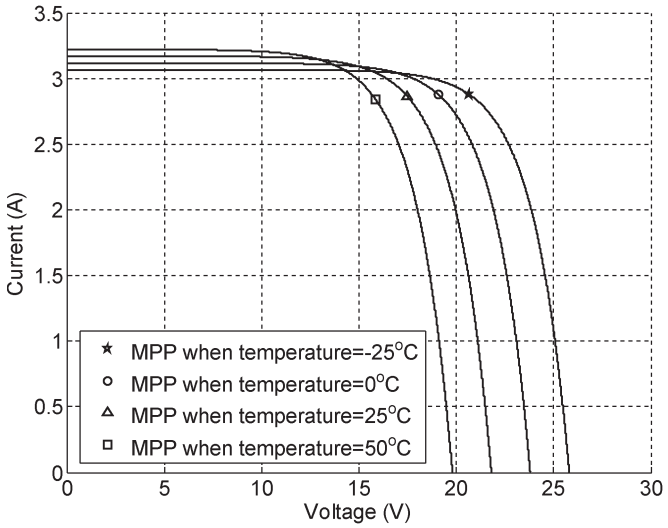

Fig. 7. Simulated I–V curves of BP350 influenced by cell temperature when the insolation is constant 1000 W/m^2.

current in a MSX-83 solar panel, to which the specification refers [19].

As shown in Figs. 6–8, both the photovoltaic voltage and the photovoltaic current at the MPP can represent the MPP. For a particular operating condition, the control of MPPT normally regulates either the voltage or current to a certain value that represents the local MPP. However, the mapping between MPP and these variables is time variant, as it is a function of changing insolation and temperature. Ideally, however, this relationship is constant or changes slowly within a range. It was determined that the photovoltaic voltage is a preferable control variable because of the advantages described below.

Changing radiation causes the photovoltaic current to vary dramatically, as illustrated in Fig. 6. The fast dynamic of insolation is usually caused by the cover of mixed rapidly moving clouds. If the photovoltaic current is used as the set point, the MPPT requires a fast dynamic to follow a wide

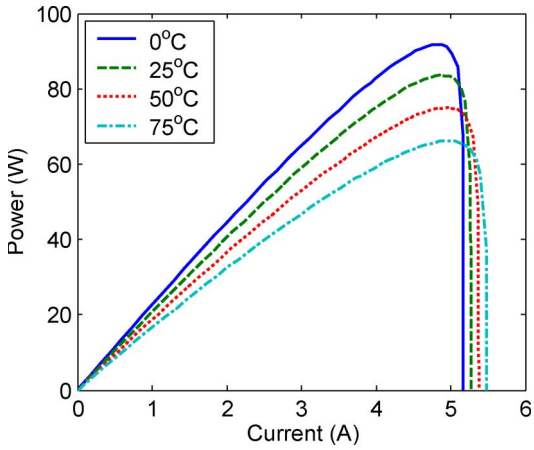

Fig. 8. Temperature effect on the relationship of power and current of MSX-83 solar panel with a constant insolation equal to 1000 W/m^2.

operating range from 0 A to the short-circuit current because the current is heavily dependant on weather conditions. In contrast, the changing insolation only slightly affects the voltage of MPP (V_{MPP}). Fig. 7 shows that the cell temperature is the dominant factor varying V_{MPP} when the temperature changes. However, cell temperature has a slow dynamic and is always within a certain range.

Unlike the current of the MPP, the photovoltaic voltage of MPP is usually bounded to 70%–82% of the open-circuit voltage. This gives the tracking range a lower bound and upper limit. When regulation of the photovoltaic voltage is implemented, the MPPT can quickly decide the initial point according to the percentage of the open-circuit voltage. Fig. 9 shows a measured start of MPPT from the open-circuit condition. The IMPPT shown in Fig. 9 represents the improved MPPT, where the initial set point of photovoltaic voltage is set to 80% of the open-circuit voltage and is close to the true V_{MPP}. The control structure of IMPPT is illustrated in Fig. 10, which will be discussed further in the following paragraphs. By comparison, the voltage regulation loop makes the starting time of MPPT much shorter than the operating time of the perturbation and observation algorithm of MPPT, the P&O method, which was introduced in [20] and [21].

The study [22] shows that the photovoltaic current value at MPP is close to about 86% of the short-circuit current. Because the photovoltaic current dramatically varies with insolation, the transient response of MPPT can occasionally cause the photovoltaic current to reach its saturation point, which is the short-circuit current. This shall be prevented because its nonlinearity causes a sudden voltage drop and results in power losses. However, for the regulation of photovoltaic voltage, the voltage saturations can be easily avoided because a controller knows the operating range is bounded about 70%–82% of the open-circuit voltage. Furthermore, a good-quality measurement of voltage signal is cheaper and easier than that of current measurement.

The resulting recommended control structure has been shown in Fig. 10, which is a general mechanism for MPPT. This control structure can use both a dc/ac MPPT module and a dc/dc MPPT module. As demonstrated in Fig. 10, the MPPT

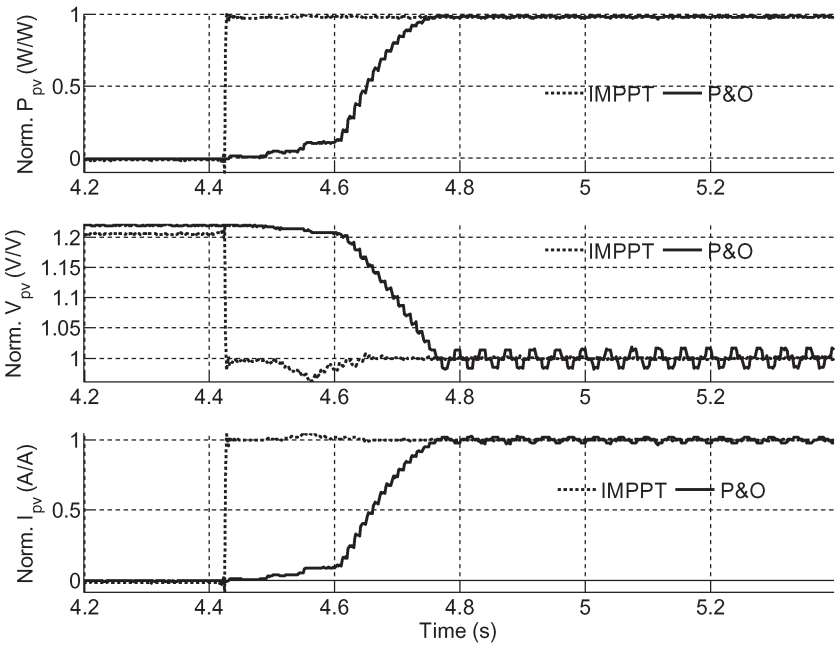

Fig. 9. Measured start of MPPT between IMPPT and P&O.

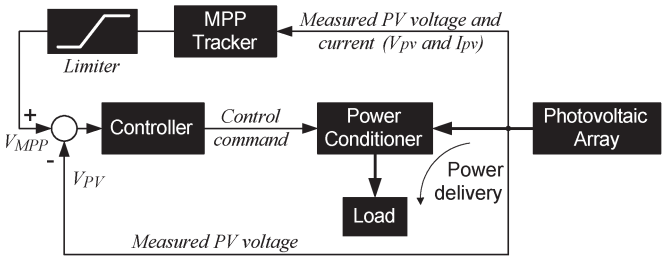

Fig. 10. Recommended control mechanism for MPPT.

is based on photovoltaic power measurement and regulation of photovoltaic voltage, so this configuration is applicable for controlling the photovoltaic interface of both stand-alone and grid-connected photovoltaic power systems. The controller regulates the photovoltaic voltage to follow a time-variant set point, which represents the voltage of optimal operating point ($V_{\rm MPP}$). The value of $V_{\rm MPP}$ is continuously tracked and updated by the MPP tracker. The limiter shown in Fig. 10 gives the tracking range a lower and upper bound.

V. Converter Topologies

This section provides a comparative study with the goal of choosing a suitable converter topology for the applications of the dc/dc MPPT modules shown in Fig. 5. Nonisolated buck and boost dc–dc converters are widely used in stand-alone photovoltaic power systems because of their simplicity and efficiency. A buck dc–dc converter, as shown in Fig. 11, has a discontinuous input current and a continuous output current before considering the input filter. On the contrary, the boost converter illustrated in Fig. 12 has a continuous input current and a discontinuous output current. These characteristics make their applications different when they are used as photovoltaic interfaces. The battery symbols in Figs. 11 and 12 represent the constant voltage of the dc bus.

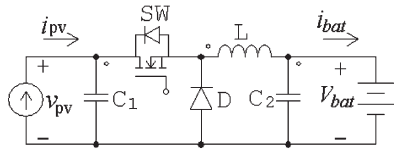

Fig. 11. Equivalent circuit of a buck dc/dc topology used as the photovoltaic power interface.

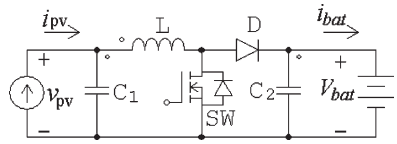

Fig. 12. Equivalent circuit of a boost dc/dc topology used as the photovoltaic power interface.

For fair comparison, the buck and boost converters are physically designed and described in following sections. They operate as the power interface between a photovoltaic module and a constant-voltage load. This paper presents two conceptual designs used for photovoltaic power interfaces to compare buck and boost topologies, as shown in Figs. 11 and 12, respectively. Aside from the output voltages, both converter designs follow the same specifications tabulated in Table II. Table III lists the symbols used in following paragraphs. For easy comparison, both the boost and buck share the same definition and symbols.

A. Component Comparison

The boost topology has some advantages over the buck for this application, which are discussed in following.

In considering the inductor in the topologies, neither shows a significant advantage over the other. To achieve the same ripple of inductor current, the boost topology needs more inductance than the buck converter, as shown in Table IV. However, the

TABLE II
DESIGN SPECIFICATIONS

Topology	Buck	Boost
Nominal input voltage	17.3V	17.3V
Maximum input voltage	24V	24V
Nominal output voltage	12V	24V
Maximum output voltage	15V	30V
Nominal solar power	50W	50W
Maximum solar power	60W	60W
Switching frequency	40kHz	40kHz
Max inductor current ripple	10%	10%
Maximum input voltage ripple	0.5%	0.5%
Maximum output voltage ripple (%)	0.5%	0.5%
Convection	Natural	Natural
Efficiency	>90%	>90%

TABLE III
LIST OF SYMBOLS

Symbol	Description
C_1	Input capacitor or capacitance
C_2	Output capacitor or capacitance
L	Inductor or inductance
I_{pv}	Steady-state photovoltaic current or input current
Δv_{pv}	Value of photovoltaic voltage ripple
f_{sw}	Switching frequency
m	Switching duty cycle
V_{bat}	Steady-state output voltage
Δi_L	Value of inductor current ripple
V_{PV}	Steady-state photovoltaic voltage
Δv	Value of output voltage ripple
I_O	Steady-state output current

TABLE IV
INDUCTANCE AND CAPACITANCE

Description	Buck	Boost
Input capacitance C_1	$\frac{I_{pv}(1-D)}{2\Delta v_{pv} f_{sw}}$ = 127.94 μF	$\frac{\Delta i_L}{8\Delta v_{pv} f_{sw}}$ = 10.44μF
Inductance L	$\frac{V(1-D)}{2\Delta i_L f_{sw}}$ = 110.3μH	$\frac{V_{PV} D}{2\Delta i_L f_{sw}}$ = 208.9μH
Output capacitance C_2	$\frac{\Delta i_L}{8\Delta v f_{sw}}$ = 21.70μF	$\frac{I_O D}{8\Delta v f_{sw}}$ = 60.58μF

rms current through the inductor is much less than that of the buck converter as shown in Table V.

In considering the input capacitors, the buck topology requires a large and expensive capacitor to smooth the discontinuous input current from the photovoltaic module, as demonstrated in Table IV, and to handle significant current ripple, as shown in Table V. On the other hand, the photovoltaic current in the boost converter current is as smooth as its inductor current,

TABLE V
RMS VALUES

Description	*Buck*	*Boost*
RMS current through input capacitor C_1	1.9311A	0.1669A
RMS current through output capacitor C_2	0.2405A	1.3041A
RMS current through MOSFET	3.4758A	1.5295A
RMS current through diode	2.3099A	2.4578A
RMS current through inductor	4.1734A	2.8948A

without any input capacitor. A small and cheap capacitor can further smooth the photovoltaic current and voltage.

For the selection of the power MOSFETs and driver, we see that the current rating is lower in the boost than in the buck topology, as illustrated in Table V. The buck converter also requires a high-side MOSFET driver, which is more complex and expensive than the low-side driver used in the boost converter.

In most applications, the photovoltaic array acts as a power source to energize devices capable of storing electricity and/or a utility grid. However, the capacity of solar generation systems depends heavily on the presence of light. At night, a current could flow back into photovoltaic cells from the bus; however, reverse current must be avoided because it causes leakage loss, extensive damage, or could even cause a fire [23]. Blocking diodes are effective to prevent reverse current flows. In the selection of blocking diodes, the boost topology shows significant advantages over the buck converter. In the boost topology, the freewheel diode can serve as the blocking diode to avoid reverse current. However, in the buck interface, the blocking diode is an additional component that is needed to conduct the full photovoltaic current. This results in an increase in cost and additional power loss due to the forward voltage drop.

B. Modeling Comparison

This section analyzes and compares the frequency characteristics of the topologies according to the parameters derived in the previous section. All symbols used in the following paragraphs refer to Table III. These are also illustrated in Figs. 11 and 12, respectively. In this system, the battery voltage $V_{\rm bat}$ is effectively a constant dc bus due to the slow dynamics of the batteries. Furthermore, the voltage change across the capacitor C_2 can be ignored. The analysis only covers the continuous inductor current mode, which is the nominal operation of the proposed dc/dc converters.

When the buck converter is used in the continuous inductor current mode, the averaged small-signal state-space model is derived as

$$\frac{d}{dt}\begin{bmatrix}\hat{i}_L\\ \hat{v}_{\rm pv}\end{bmatrix} = \begin{bmatrix}-\frac{R_L}{L} & \frac{m}{L}\\ -\frac{m}{C_1} & \frac{1}{r_{\rm pv}C_1}\end{bmatrix}\begin{bmatrix}\hat{i}_L\\ \hat{v}_{\rm pv}\end{bmatrix} + \begin{bmatrix}\frac{v_{\rm pv}-V_{\rm FW}}{L}\\ -\frac{i_L}{C_1}\end{bmatrix}\hat{m} \quad (1)$$

$$\hat{y} = [0 \quad 1]\begin{bmatrix}\hat{i}_L\\ \hat{v}_{\rm pv}\end{bmatrix} \quad (2)$$

according to the state-space averaging method. m denotes the duty ratio of switching, $m' = 1 - m$, $\hat{m}$ symbolizes the small increment of the duty ratio m, and $\hat{m}'$ represents the small increment of m'. Without loss of generality, the nonlinear

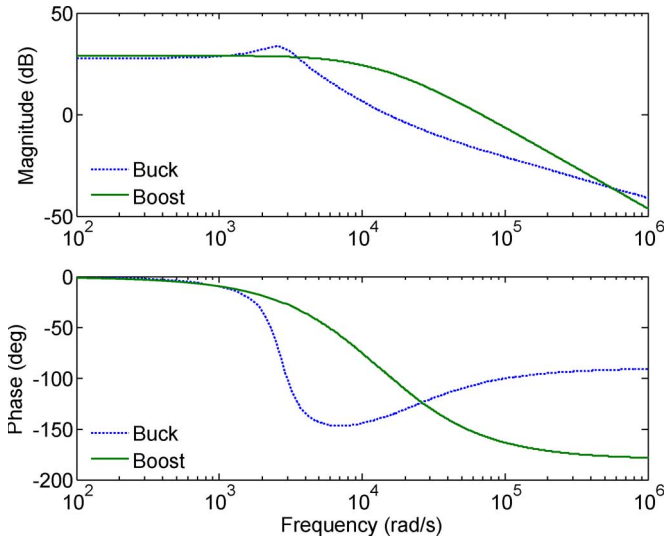

Fig. 13. Bode diagram of buck and boost topologies under nominal operating condition.

relationship of photovoltaic voltage and current represented by $r_{\rm pv}$ is a dynamic resistance that is defined as

$$r_{\rm pv} = \frac{\hat{v}_{\rm pv}}{\hat{i}_{\rm pv}} \tag{3}$$

where $\hat{v}_{\rm pv}$ represents the small increment of photovoltaic voltage, and $\hat{i}_{\rm pv}$ represents the small increment of photovoltaic current. The linearization process is based on a model that is linear in the incremental components of inputs and outputs around a chosen operating point.

Similarly, the averaged small-signal state-space model can be formulated as

$$\frac{d}{dt}\begin{bmatrix}\hat{i}_L \\ \hat{v}_{\rm pv}\end{bmatrix} = \begin{bmatrix}-\frac{R_L}{L} & \frac{1}{L} \\ -\frac{1}{C_1} & \frac{1}{r_{\rm pv}C_1}\end{bmatrix}\begin{bmatrix}\hat{i}_L \\ \hat{v}_{\rm pv}\end{bmatrix} + \begin{bmatrix}-\frac{V_{\rm bat}-V_{FW}}{L} \\ 0\end{bmatrix}\hat{m}' \tag{4}$$

$$\hat{y} = \begin{bmatrix}0 & 1\end{bmatrix}\begin{bmatrix}\hat{i}_L \\ \hat{v}_{\rm pv}\end{bmatrix} \tag{5}$$

when the boost converter is used as the interface. The dynamic resistance $r_{\rm pv}$ is in fact a time-variant parameter that depends on operating conditions.

By analyzing the mathematical model of the buck interface (1), there are four time-variant parameters including the switching duty cycle m, the photovoltaic voltage $v_{\rm pv}$, the inductor current i_L, and the dynamic resistance $r_{\rm pv}$. However, when the boost topology is used for photovoltaic interface, there is only one time-variant parameter $r_{\rm pv}$, which is shown in (4); thus, there are less time-variant factors in the mathematical model when the boost converter is used as the photovoltaic interface.

Based on the parameters derived in Table IV and the nominal operating condition, the system frequency response can be illustrated by a Bode diagram, as shown in Fig. 13. We can also compute the poles and zeros of the models of buck and boost topology and plot them in the complex plane, as shown in Figs. 14 and 15, respectively. The important parameters are summarized in Table VI, which include the undamped natural frequency, damping factors, percentage of overshoot, pole locations, etc. The system with a buck topology shows

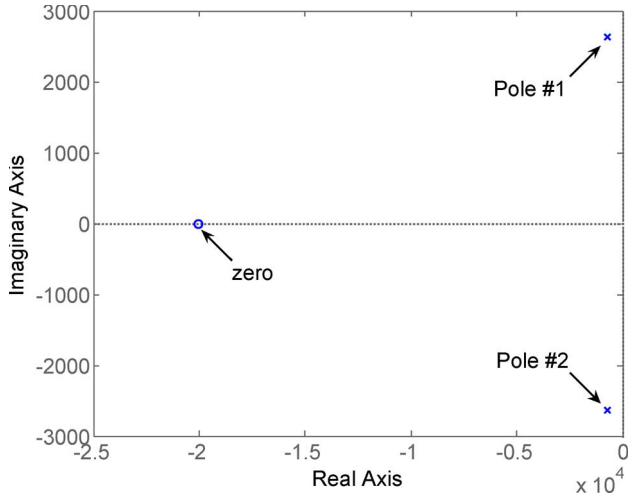

Fig. 14. Pole and zero locations of the system using buck topology.

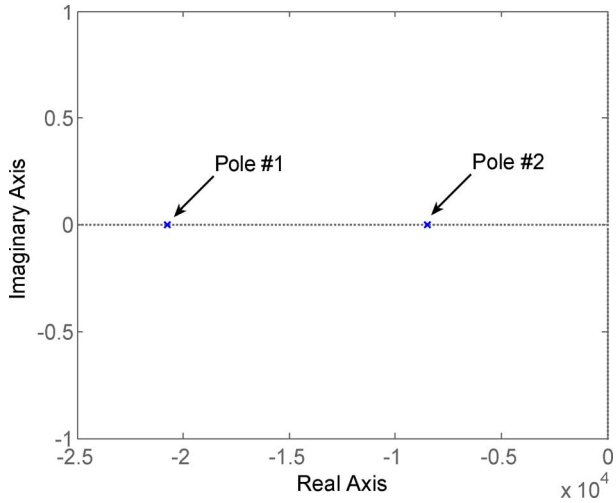

Fig. 15. Pole locations of the system having boost topology.

a pair of complex-conjugate poles and a light damping factor of 0.266. By comparison, the boost topology demonstrates a well-damped characteristic, where the damping factor is equal to one. The lightly damped system is a difficult control problem, as described in [24]. In comparing the undamped natural frequency, we see that the boost interface shows better dynamic characteristics than the buck interface. Generally, we can see advantages in terms of a wider bandwidth and smaller resonance due to the small input capacitance of the boost converter.

VI. Conclusion

This paper has discussed the topologies used for photovoltaic power systems to optimize the operation of MPPT. First, it illustrated that nonideal conditions considerably downgrade the performance of MPPT, especially when photovoltaic modules are connected in series. To solve this problem, this paper proposed an individual power interface for each photovoltaic module and recommended a structure suitable for the photovoltaic features and MPPT to minimize the performance reduction caused by nonideal conditions. Fig. 5 shows the recommended grid-connected topology with UPS function.

TABLE VI
COMPARISON OF SYSTEM PARAMETERS BETWEEN BUCK AND BOOST TOPOLOGIES

System parameters	Buck	Boost
Undamped Natural frequency	2.73×10^3 rad/s	1.33×10^4 rad/s
Damping factor	0.266	1.0
Overshoot of unit step response	42%	0%
Poles	$-726\pm j2.63\times10^3$	-8.49×10^3 and -2.07×10^4
Zeros	2×10^4	n/a

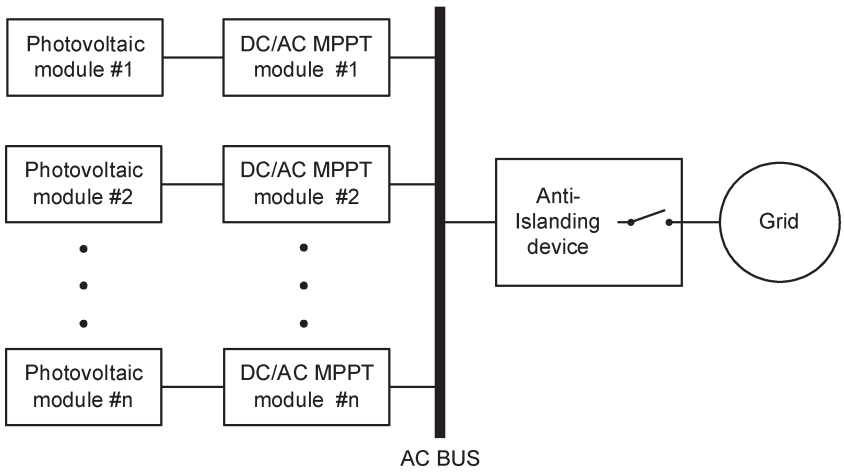

Fig. 16. Topology of grid-connected photovoltaic power systems with an ac bus configuration.

For high-efficiency conversion, most grid-connected power systems ignore dc/dc modules and convert dc photovoltaic energy directly to ac grid power. Fig. 16 illustrates a different photovoltaic power configuration, which consists of dc/ac MPPT modules, an ac voltage bus, and an anti-islanding device, where the bus voltage is equal to the grid voltage. The dc/ac MPPT module is the power interface between the photovoltaic module and the ac voltage bus. This is controlled by the algorithm of MPPT to generate the maximum possible solar power. The energy is eventually transferred to the grid via the ac bus and anti-islanding device. As shown in Figs. 5 and 16, both mechanisms ensure that any defective photovoltaic module will not influence the overall array so that each individual module is able to work at its optimal operating point.

The control variable that represents the MPP can be either the photovoltaic voltage or the photovoltaic current. An analysis shows that regulating the photovoltaic voltage has advantages to improve the performance of MPPT. Finally, this paper provides a comparative study to choose the right converter topology for the applications of dc/dc MPPT modules. The boost topology shows some advantages over the buck converter for this application. The features include cheaper implementations and better dynamic response when compared to the buck converter.

REFERENCES

[1] *Total photovoltaic power installed in IEA PVPS countries*. (2005, Oct.). [Online]. Available: http://www.iea-pvps.org/isr/22.htm
[2] *Timeline of solar cells*. (2007, Mar.). [Online]. Available: http://en.wikipedia.org/wiki/Timeline_of_solar_cells
[3] *Germany—BIPV Case Studies*. (2007, Mar.). [Online]. Available: http://www.cler.org/predac/article.php3?id_article=511
[4] *Solar Energy Technologies Program*. (2006, Oct.). [Online]. Available: http://www.eere.energy.gov/RE/solar_photovoltaics.html
[5] *Photovoltaic Timeline*. (2007, Mar.). [Online]. Available: http://www.eia.doe.gov/kids/history/timelines/photovoltaics.html
[6] M. R. Patel, *Wind and Solar Power Systems*. Boca Raton, FL: CRC Press, 1999.
[7] Fronius, *Reaction to Non-Optimal Conditions*. (2006, Oct.). [Online]. Available: http://www.fronius.com/worldwide/usa.solarelectronics/downloads/fronius_ig_reaction_to_non_optimal_conditions.pdf
[8] B. M. T. Ho and H. S.-H. Chung, "An integrated inverter with maximum power tracking for grid-connected PV systems," *IEEE Trans. Power Electron.*, vol. 20, no. 4, pp. 953–962, Jul. 2005.
[9] T. Shimizu, O. Hashimoto, and G. Kimura, "A novel high-performance utility-interactive photovoltaic inverter system," *IEEE Trans. Power Electron.*, vol. 18, no. 2, pp. 704–711, Mar. 2003.
[10] E. Roman, P. Ibanez, S. Elorduizapatarietxe, R. Alonso, D. Goitia, and I. M. de Alegria, "Intelligent PV module for grid-connected PV systems," in *Proc. 30th Annu. Conf. IEEE Ind. Electron. Soc.*, Busan, Korea, pp. 3082–3087.
[11] FSEC, *Evaluation of Shading on ASE Americas ASE-300-DGF/50 Photovoltaic Module*. (2006, Oct.). [Online]. Available: www.fsec.ucf.edu/PVT/Resources/publications/pdf/ASESHADINGTESTS.PDF
[12] M. Veerachary, T. Senjyu, and K. Uezato, "Maximum power point tracking of coupled inductor interleaved boost converter supplied PV system," *Proc. Inst. Electr. Eng.—Electric Power Applications*, vol. 150, no. 1, pp. 71–80, Jan. 2003.
[13] E. Roman, R. Alonso, P. Ibanez, S. Elorduizapatarietxe, and D. Goitia, "Intelligent PV module for grid-connected PV systems," *IEEE Trans. Ind. Electron.*, vol. 53, no. 4, pp. 1066–1073, Jun. 2006.
[14] *50 Watt Photovoltaic Module—BP350*. (2003, Aug.). [Online]. Available: http://www.rfindustries.com.au/rfiproducts/solar/BP350U_v2.pdf
[15] SMA, *Sunny Boy Inverters*. (2006, Oct.). [Online]. Available: http://www.sma-america.com/sb2500.html
[16] Xantrex, *GT Series Grid Tie Solar Inverters*. (2006, Nov.). [Online]. Available: http://www.xantrex.com/web/id/172/p/1/pt/25/product.asp
[17] *IEEE Recommended Practice for Utility Interface of Photovoltaic (PV) Systems*, IEEE Std 929-2000, Jan. 2000.
[18] *UL Standard for Inverters, Converters, Controllers and Interconnection System Equipment for Use with Distributed Energy Resources*, UL 1741, Nov. 2005.

[19] Solarex, *MSX-77 and MSX-83 Photovoltaic Modules*. (1999, Jul.). [Online]. Available: http://www.windpower.com.au/download/msx77-83.pdf
[20] E. Koutroulis, K. Kalaitzakis, and N. C. Voulgaris, "Development of a microcontroller-based, photovoltaic maximum power point tracking control system," *IEEE Trans. Power Electron.*, vol. 16, no. 1, pp. 46–54, Jan. 2001.
[21] N. Femia, G. Petrone, G. Spagnuolo, and M. Vitelli, "Optimization of perturb and observe maximum power point tracking method," *IEEE Trans. Power Electron.*, vol. 20, no. 4, pp. 963–973, Jul. 2005.
[22] M. A. S. Masoum, H. Dehbonei, and E. F. Fuchs, "Theoretical and experimental analyses of photovoltaic systems with voltage and current-based maximum power-point tracking," *IEEE Trans. Energy Convers.*, vol. 17, no. 4, pp. 514–522, Dec. 2002.
[23] J. C. Wiles and D. L. King, "Blocking diodes and fuses in low-voltage PV systems," in *Proc. 26th IEEE Photovoltaic Spec. Conf.*, Sep. 29–Oct. 3, 1997, pp. 1105–1108.
[24] G. C. Goodwin, S. F. Graebe, and M. E. Salgado, *Control System Design*. Upper Saddle River, NJ: Prentice-Hall, 2001.

Weidong Xiao (S'03) received the M.A.Sc. degree in electrical engineering from the University of British Columbia, Vancouver, BC, Canada, in 2003. He is currently working toward the Ph.D. degree at the University of British Columbia.

His fields of research involve power electronics and applications of renewable energy sources.

Nathan Ozog (S'06) received the B.A.Sc. degree in electrical engineering from the University of British Columbia (UBC), Vancouver, BC, Canada, in 2006. He is currently working toward the M.A.Sc. degree in the Power Simulation Laboratory, UBC.

His research interests are in power system simulation, alternative energy sources, and infrastructure interdependencies.

William G. Dunford (S'78–M'81–SM'92) received the degree in engineering from Imperial College, London, U.K., and the Ph.D. degree from the University of Toronto, Toronto, ON, Canada.

He was part of a team that modeled satellite batteries at Alcatel, Toulouse, France. He is currently with the Clean Energy Centre, University of British Columbia, Vancouver, BC, Canada. He has worked on photovoltaic applications for a number of years. His other interests include distributed systems, in general, with particular emphasis on efficiency, power quality, and automotive applications.

Dr. Dunford was the General Chair of the IEEE Power Electronics Specialists Conference in 1986 and 2001.